

# Effect of Vibration Direction on Vibration-Assisted Fixed Abrasive Polishing

Ruikun NIU\*, Huantao WANG\*\*, Zhongming WU\*\*\*, Li SUN\*\*\*\*

\*Jinling Institute of Technology, Nanjing 211169, Jiangsu, China, E-mail: nrk5204@jit.edu.cn (Corresponding author)

\*\*Jinling Institute of Technology, Nanjing 211169, Jiangsu, China

\*\*\*Jinling Institute of Technology, Nanjing 211169, Jiangsu, China

\*\*\*\*Jinling Institute of Technology, Nanjing 211169, Jiangsu, China

<https://doi.org/10.5755/j02.mech.34089>

## 1. Introduction

Vibration-assisted solidified abrasive polishing is a composite processing method combining solidified abrasive polishing and ultrasonic vibration, which combines the advantages of solidified abrasive polishing and vibration-assisted processing [1, 2]. By using the regular impact, scratching and cavitation of ultrasonic vibration, the contact between the abrasive grain and the workpiece surface becomes indirect, and the intermittent contact can effectively reduce the friction between the abrasive grain and the workpiece surface, reduce the generation of scratches on the workpiece surface, and reduce the action time of the abrasive grain on the processing area, which can improve the processing efficiency of solidified abrasive processing and the workpiece surface quality [3, 4]. Among the vibration parameters of vibration-assisted polishing, the influence of vibration mode on the processing effect of the workpiece is very important, and the depth of penetration of abrasive grains, the impact of abrasive grains on the workpiece and the mechanism of slip-friction during processing under different vibration modes will change, which affects the surface quality and processing efficiency of the processed workpiece.

Yang et al. proposed a technique of ultrasonic elliptical vibration-assisted solidified abrasive polishing of silicon wafers, and found that elliptical vibration-assisted polishing improved the stability of polishing and the surface morphology of the workpiece [5, 6]. Li et al. conducted simulation and validation experiments on vibration-assisted polishing of single abrasive grains and showed that vibration-assisted polishing can improve material removal efficiency [7]. Chen et al. conducted ultrasonic elliptical vibration-assisted polishing experiments and obtained the optimal process parameters that can obtain better quality fiber array endfaces with elliptical vibration assistance [8, 9]. Guo et al. explored vibration-assisted magnetic polishing of rectangular microstructures, and the processed rectangular microstructures ensured both the form of microscopic features and obtained better surface quality [10, 11]. Yu et al. investigated axial vibration. The results showed that axial vibration-assisted polishing improved the machining quality and efficiency [12, 13]. Kobayashi et al. conducted an experimental study on ultrasonic elliptical vibration polishing of silicon wafer edges and found that the workpiece obtained better surface quality under elliptical vibration [14, 15]. Xu et al. used two-dimensional vibration-assisted polishing of sapphire substrates in horizontal and vertical directions and showed that two-dimensional vibration-assisted polishing

improved processing efficiency and processing quality [16].

The above-mentioned research results show that vibration-assisted can affect the quality and efficiency of polishing processing, so in order to investigate the mechanism of vibration direction on solidified abrasive polishing, this paper establishes a model of single abrasive vibration-assisted solidified abrasive processing calcium fluoride crystals, analyzes the effect of individual vibration direction on the surface morphology cloud, profile depth, stress, and strain of the workpiece, and carries out the solidified abrasive polishing without vibration, axial and radial vibration modes. Validation experiments on polishing calcium fluoride crystals without vibration, axial and radial vibration.

## 2. Simulation of vibration-assisted solidification abrasive polishing of single abrasive grains

### 2.1. Simulation model building and result extraction

In order to simplify the model and process of simulation, the following assumptions are made.

1. Intercept a small section of material on the workpiece to simulate the machining process; ignore the effect of polishing fluid and cavitation on the machining process.

2. The motion of the abrasive grain is simplified to a linear motion; the hardness of the calcium fluoride crystal is much lower than that of the abrasive grain, and the abrasive grain is simplified to a rigid body.

3. Converting the force exerted on the workpiece by the pressure system to the abrasive grain; the workpiece is self-transmitted in the actual machining, and the workpiece is now assumed to be relatively stationary.

Fig. 1 shows a schematic diagram of vibration-assisted solidified abrasive processing with a single abrasive grain. Without considering the abrasive grain shedding, the abrasive grain is always solidified on the surface of the polishing pad and only scratches the surface of the workpiece with the rotation of the pad. The abrasive grain has a specific frequency, amplitude and direction of vibration.

Fig. 2 shows the geometric model for the simulation of vibration-assisted solidification abrasive processing of a single abrasive grain. The shape of the abrasive grain is set as a positive octahedron with a diagonal length of 5  $\mu\text{m}$ , and the workpiece is a rectangular body of 30  $\mu\text{m}$  in length, 5  $\mu\text{m}$  in width and 10  $\mu\text{m}$  in height. The workpiece is set as a deformable entity, and a hexahedral mesh structure is adopted to ensure the computational accuracy. In order to simulate the real machining state, the front surface of the workpiece is set as XOY symmetry surface, the two sides

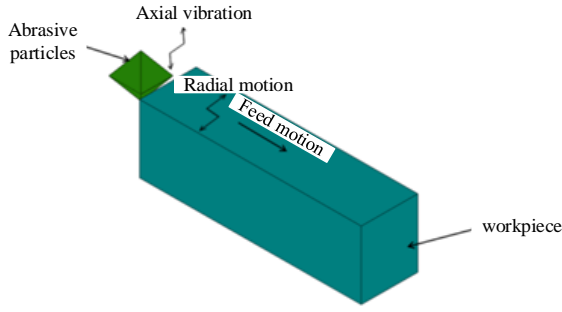


Fig. 1 Schematic diagram of vibration-assisted solidification abrasive processing of single abrasive grains

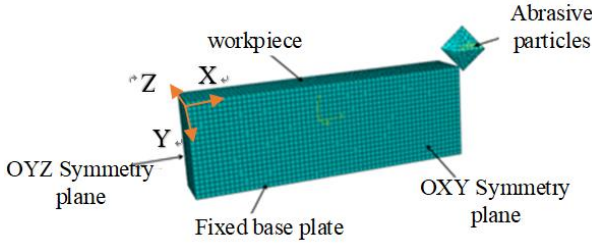


Fig. 2 Geometric model of vibration-assisted solidification abrasive processing of single abrasive grains

are set as YOZ symmetry surface, and the bottom surface is set as completely fixed surface to ensure the stability of the model calculation.

The unit of length is mm, the unit of time is s, the unit of force is N, the unit of density can be derived as  $\text{ton}/\text{mm}^3$ , the unit of mass is ton, the unit of pressure is MPa, and the acceleration is  $\text{mm}/\text{s}^2$ . Due to the small cutting depth, calcium fluoride crystals are processed mainly by plastic removal, which is simplified to an ideal elasto-plastic material for the simulation study. This simulation model is set with reference to its material properties, and the elastic anisotropy of the calcium fluoride material is expressed using the stiffness coefficient according to the elastic mechanics. In the actual solidified abrasive polishing, when the pressure is constant and no vibration is applied, there exists a constant

depth of cut of the abrasive grain to the workpiece, and the grain is moved to a constant depth of cut  $\delta$  at the right side face edge of the workpiece during assembly. Load setting: The speed is applied to the abrasive grain to make it move forward at a constant speed, while at the same time vibrations of a specific direction, frequency and amplitude are applied. The speed of uniform linear motion is obtained from the spindle speed and the position of the polishing pad where the abrasive grain is located.

$$f(x) = A \sin(2\pi ft), \tag{1}$$

$$f(x) = B \sin(2\pi ft), \tag{2}$$

where  $A, B$  are amplitudes in different directions (they can be in X direction, Y direction or Z direction based on the vibration directions).  $f$  is the frequency of the vibration. The basic parameters of the model are set as in Table 1.

## 2.2. Analysis of simulation results

### 2.2.1. Surface morphology cloud diagram

Fig. 3 shows the surface morphology of the workpiece under different vibration directions (the unit here is mm), the surface morphology of the workpiece changes uniformly under the condition of no vibration, and the craters are small; the surface morphology of axial vibration changes the most, and the machined area is depressed in the Y direction due to the extrusion of the abrasive grains on the workpiece, while the surface morphology of the unmachined area is raised due to the indirect extrusion. The surface morphology of radial vibration fluctuates more, the craters on the surface become bigger, and the abrasive grains have larger deformation at the positive and negative peaks of vibration and when cutting away from the surface of the workpiece, but in general, the difference between the surface morphology of the workpiece after processing in radial vibration and vibration-free mode is not big, and the surface morphology is better.

Table 1

Basic parameters of vibration-assisted solidification abrasive processing simulation

Simulation conditions	Depth of penetration ( $\delta/\mu\text{m}$ )	Diagonal length ( $\mu\text{m}$ )	Frictional coefficient	Amplitude ( $\mu\text{m}$ )	Frequency (kHz)
Parameter	0.5	5	0.3 [2]	1	40

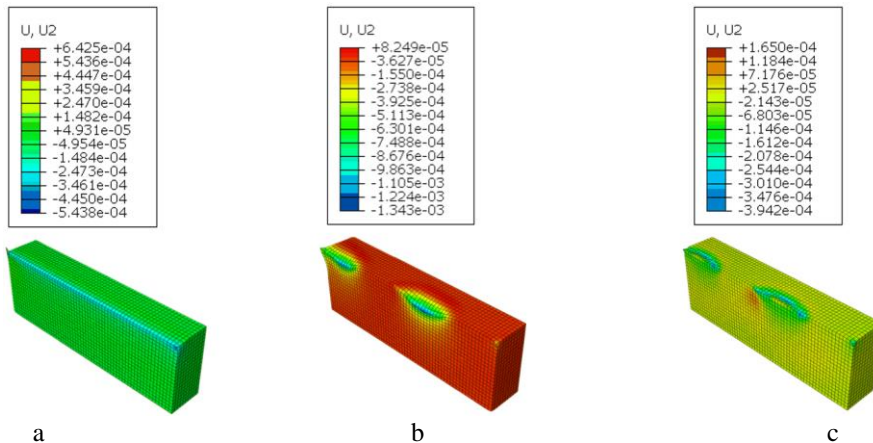


Fig. 3 Cloud map of surface morphology of workpiece under different vibration modes: a - no vibration; b - axial vibration; c - radial vibration

### 2.2.2. Profile depth

Fig. 4 shows the profile depth of the workpiece in Y-direction under different vibration directions. The profile depth of axial vibration is the largest, and the profile depth of radial vibration is slightly larger than that of no vibration. Because of the axial impact of axial vibration, the penetration depth of abrasive particles of axial vibration is much larger than that of radial vibration and no vibration, so its profile depth peak is the largest and the surface morphology changes obviously. Due to the scratching effect of radial vibration on the surface of the workpiece, the surface of the workpiece is loosened, so that the depth of penetration of the abrasive grains of radial vibration is slightly greater than that of no vibration.

### 2.2.3. Residual stress

Fig. 5 shows the residual stresses on the workpiece surface under different vibration directions. The workpiece is subjected to tensile stress when the value of residual stress is positive, and the larger the value of tensile stress, the easier the workpiece is to be destroyed. The residual stresses on the surface of the workpiece after processing in three different vibration directions are all compressive stresses, among which the residual stresses generated in the axial vibration mode are the largest, the residual stresses on the workpiece after processing without vibration are the smallest and fluctuate little, and the residual stresses on the workpiece after processing in the radial vibration mode are greater than those without vibration on the whole. Therefore, the workpiece may be subjected to greater polishing pressure in the axial vibration mode, which increases the surface depth of cut of the abrasive grains on the workpiece, while the surface depth of cut in the radial vibration mode may be slightly greater than that without vibration.

### 2.2.4. Strain

Fig. 6 shows the strain diagram of the workpiece surface under different vibration directions. It can be seen

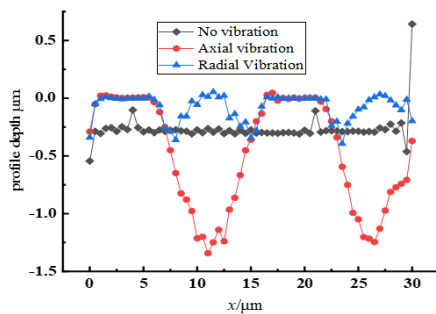


Fig. 4 Depth of profile for different vibration directions

that the workpiece strain under the radial vibration mode is the smallest, the no vibration is slightly larger than the radial vibration, and the workpiece strain under the axial vibration mode is the largest. The strain distribution of the workpiece in the radial vibration mode is more uniform, and the strain value fluctuates above and below 0 with very small changes, while the strain distribution of the workpiece in the axial vibration mode is not uniform, and large craters and bumps appear on the workpiece surface.

The results of surface morphology clouds, profile depth, residual stress and strain for different vibration directions assisted solidified abrasive polishing can be concluded as follows:

The surface morphology change, profile depth, residual stress and strain of the workpiece after axial vibration-assisted polishing are the largest, so the axial vibration can promote more material removal by abrasive grains, and the material removal rate may be larger; the profile depth and strain of radial vibration-assisted polishing are slightly larger compared with no vibration, so the material removal rate may be slightly larger than that of vibration-free polishing, where as the abrasive grains under radial vibration will have periodic Slip rubbing, on the one hand, may reduce the generation of scratches on the workpiece surface, on the other hand, the periodic slip rubbing can make the workpiece surface loose, and the material on the workpiece surface may be easier to remove, compared with vibration-free polishing, may be able to effectively remove the workpiece surface defects, so the surface quality of the workpiece after radial vibration polishing may be the best.

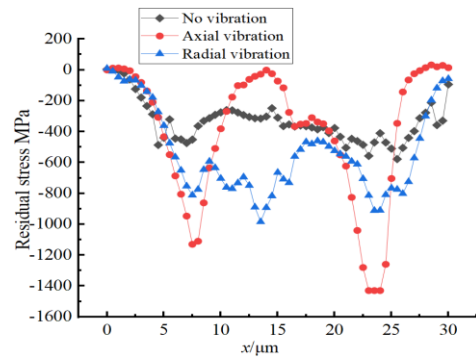


Fig. 5 Residual stresses on the workpiece surface under different vibration directions

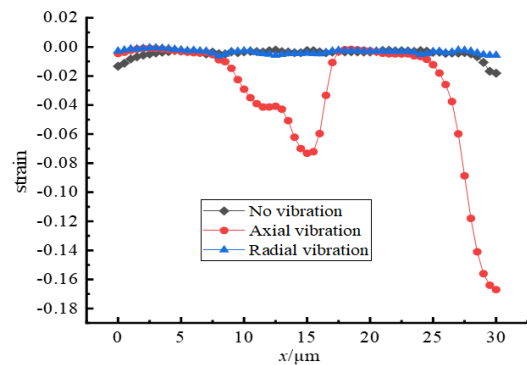


Fig. 6 Strain diagram of the workpiece surface under different vibration directions

In summary, axial vibration-assisted polishing may improve the processing efficiency; the workpiece after radial vibration-assisted polishing may obtain better surface quality.

## 3. Vibration-assisted solidification abrasive polishing experiments

Experimental studies on the effects of vibration-free, axial and radial vibration on vibration-assisted solidified abrasive polishing of calcium fluoride crystals were carried out on a planar precision ring polishing machine, where

ultrasonic vibration was provided by a designed transducer. The vibration-assisted solidified abrasive polishing system consisted of an ultrasonic generator, vibration equipment, solidified abrasive polishing pad and polishing fluid supply device. The transducer includes a matching layer (aluminum material) and a piezoelectric vibrator (annular piezoelectric vibrator). A layer of epoxy glue is coated on the bottom surface of the inner cavity of the matching layer which is bonded together with the piezoelectric vibrator, as shown in Fig. 7.

The experimental parameters were set as shown in Table 2, including spindle speed of ring polishing machine, rotational speed of bottom plate of ring polishing machine, polishing fluid flow, and pressure (acting on the workpiece). The diameter of the workpiece was 25 mm, the material was calcium fluoride crystals, the abrasive grains in the polishing pad were diamond particles with a particle size of 3-5  $\mu\text{m}$ , the pH of the polishing solution was 9, the amplitude of the axial and radial vibration was 1  $\mu\text{m}$ , and the frequency was 40 kHz. the polishing pad was trimmed before each polishing to achieve a consistent polishing effect; before polishing, the workpiece would be ground under the same conditions to achieve The original thickness of the workpiece was measured using a spiral micrometer before polishing, and the mass of the workpiece was measured several times after polishing using a Sedolis BS224S precision balance and averaged; the surface quality and morphology of the workpiece were observed using an optical microscope, and the surface roughness of the polished calcium fluoride crystals was measured using a CSPM4000 scanning probe microscope.

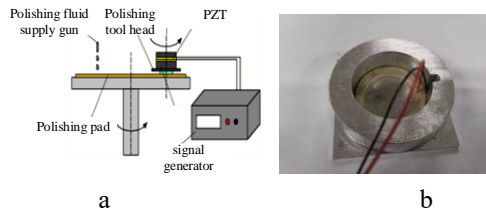


Fig. 7 Schematic diagram of vibration-assisted solidified abrasive polishing: a - overall unit; b - transducer

Table 2  
Experimental parameters of vibration-assisted polishing of calcium fluoride crystals

Spindle speed (r/min)	Lower disc speed (r/min)	Polishing fluid flow rate (ml/min)	Pressure (kPa)	Polishing fluid
42	40	60	6	Deionized water

According to the quality change before and after processing, the material removal rate number was calculated as shown in Eq. (3).

$$MRR = \frac{\Delta m \times h_0}{M_0 \times t} \times 10^6 \text{ nm/min}, \quad (3)$$

where  $MRR$  is the material removal rate of the workpiece after machining (in  $\text{nm}/\text{min}$ );  $\Delta m$  is the mass difference before and after machining (in  $\text{g}$ );  $M_0$  is the initial weight of the workpiece (in  $\text{g}$ );  $h_0$  is the initial height of the workpiece (in  $\text{mm}$ );  $t$  is the time used to machine the workpiece (in  $\text{min}$ ).

### 3.1. Surface morphology

Fig. 8 shows the surface morphology of the workpiece after polishing in different vibration directions, there are obviously many pits and scratches of different sizes in Fig. 8, a, and a large number of pits and net-like scratches are distributed on the whole workpiece surface. After the abrasive grains remove the raised part of the workpiece surface, they will continue to slip and rub the workpiece surface, and as the number of times of abrasive grains rubbing the workpiece surface increases, the scratches on the workpiece surface will increase, and thus the surface shape of the workpiece will deteriorate. In Fig. 8, b, it can be seen that there are only a few pits on the surface of the workpiece and the scratches are obviously reduced, but compared with Fig. 8, a, the depth and width of the few scratches on the surface of the workpiece become larger. At the same time, the abrasive grains will intermittently reduce the depth of cutting into the workpiece surface under the action of axial vibration, which will also reduce the accumulation of scratches on the workpiece surface, thus improving the surface quality of the workpiece to a certain extent. Fig. 8, c shows that there are fewer pits and scratches, and the depth and width of scratches are smaller. In the radial vibration mode, there is periodic scratching between the abrasive grains and the workpiece surface, and there is no impact effect with the workpiece surface. The surface quality of the workpiece can be effectively improved.

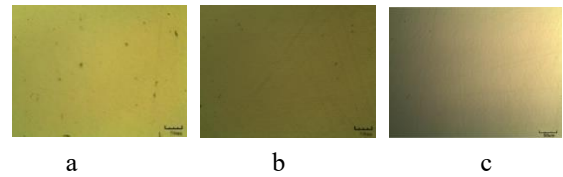


Fig. 8 Surface morphology of polished workpiece under different vibration directions: a - no vibration; b - axial vibration; c - radial vibration

### 3.2. Material removal rate

Fig. 9 shows the material removal rate of the workpiece polished under different vibration directions. The material removal rate of the workpiece polished with the aid of axial vibration is the largest, 462  $\text{nm}/\text{min}$ , which is 27.6% higher than that of the no-vibration method. The material removal rate was 384  $\text{nm}/\text{min}$  in the radial vibration mode, which increased by 6.1% compared with the no vibration mode. In the axial vibration mode, there is a periodic impact between the workpiece surface and the abrasive grains,

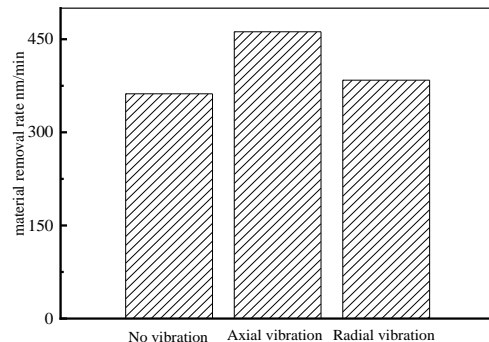


Fig. 9 Material removal rate of workpiece polished under different vibration directions

which increases the depth of cut of the abrasive grains; at the same time, it also leads to the spreading of the cracks on both sides of the entry point and loosens the surface, and the scratching effect of the abrasive grains on the workpiece surface increases the amount of material removed from the workpiece surface, thus the volume of material removed from the workpiece surface becomes significantly larger. In the radial vibration mode, the abrasive grains have a periodic scratching effect with the workpiece surface perpendicular to the feeding direction, and the workpiece surface will be softened and the material layer to be removed will be loosened, although the depth of cut of the abrasive grains is basically the same as that of the non-vibration mode, the abrasive grains will remove the workpiece surface material more easily, thus the material removal from the workpiece surface will be increased compared with the non-vibration mode.

### 3.3. Surface roughness

Fig. 10 shows the surface roughness of the workpiece after polishing with solidified abrasives in different vibration directions. It can be seen that the surface roughness  $S_a$  value of the workpiece after polishing without vibration is 7.14 nm, which is the largest under the three vibration modes, and it can be seen from Fig. 10 that the pits existing at the beginning of the workpiece surface are not effectively removed, while the surface of the workpiece is distributed with mesh-type scratches. The surface roughness  $S_a$  of the workpiece after axial vibration assisted polishing is 4.07 nm, which is 43% lower than that without vibration, and it is clear from Fig. 4 and Fig. 9 that the removal rate of polishing material under axial vibration is the largest, and the depth of abrasive grains cutting into the workpiece is large, so most of the pits on the workpiece surface can be effectively removed by the abrasive grains in the polishing pad, and the scratches distributed on the workpiece surface are also reduced, and the surface roughness of the workpiece is obviously improved. After radial vibration-assisted polishing, the workpiece surface craters are basically all effectively removed, and there are no obvious scratches on the surface, and the surface roughness  $S_a$  value is 2.87 nm, which is 59.8% lower than that without vibration, because under radial vibration, there is only periodic slip friction between the abrasive grains and the workpiece surface, and there is no impact effect under the axial vibration mode, so that the abrasive grains can effectively remove the surface craters and bumps.

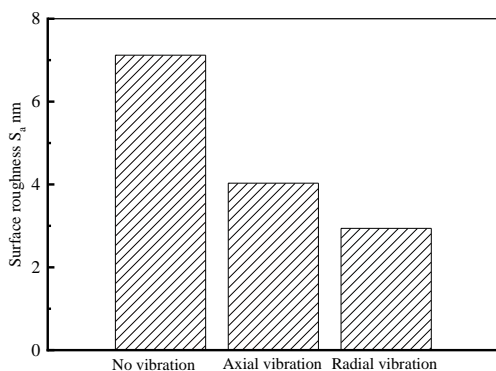


Fig. 10 Surface roughness of the workpiece after polishing under different vibration directions

At the same time, it will not produce new craters or increase the depth and width of the original craters due to the impact effect, so the surface roughness value of the workpiece is obviously reduced.

From the comparison of surface morphology and surface roughness, it can be seen that the surface quality obtained by radial vibration-assisted polishing is better, followed by axial vibration polishing, and the overall surface quality obtained by vibration-assisted polishing is better than that of vibration-free polishing; from the comparison of material removal rate, it can be seen that the solidified abrasive polishing process under axial vibration is the most efficient.

### 3.4. Comparison of experimental results and simulation results

In the above simulation results, it is analyzed that the surface shape, profile depth and strain of the workpiece under axial vibration polishing are the largest, which is consistent with the largest effect of axial vibration polishing on the material removal rate of the workpiece; while the surface scratches of the workpiece are less and the defects on the surface of the workpiece are effectively removed due to the periodic slip and rub effect under radial vibration, which is consistent with the experimental results that the surface quality after radial vibration-assisted polishing is superior.

## 4. Conclusions

In this paper, a model of single grain vibration-assisted solidification abrasive polishing calcium fluoride crystals was established, the influence mechanism of different vibration modes on the polishing effect was analyzed, and the verification experiments of vibration-assisted solidification abrasive polishing under different vibration modes were carried out, and the influence law of different vibration modes on the processing effect of vibration-assisted solidification abrasive polishing was obtained through summary and analysis. The following conclusions were drawn.

1. The material removal rate of the workpiece during axial vibration-assisted polishing is much greater than that of radial vibration and no vibration; the surface roughness value of the workpiece after radial vibration-assisted polishing is the smallest and the surface quality is the best.
2. The analysis and speculation of the simulation results are verified in the experiment, and the simulation results are highly reliable.
3. The vibration direction has an important influence on the processing effect of vibration-assisted solidified abrasive polishing, the influence of axial vibration on the processing efficiency is very significant, while the radial vibration greatly improves the surface quality of the vibration-assisted solidified abrasive polished workpiece, and this influence law has an important guiding significance for the design of process parameters in vibration-assisted polishing.

## Acknowledgments

The research is funded by High-level talent research start-up fund of China (jit-6-202117).

## References

1. Huang, J.Y.; Li, J.; Wang, J. J. et al. 2019. Vibration-

- assisted fixed abrasive polishing CaF<sub>2</sub> crystal. *Diamond & Abrasives Engineering*, 39(1): 41-46.  
<http://dx.doi.org/10.16080/j.issn1671-33x.2013.16.048>.
2. **Liang, Z.Q.; Wang, X.B.; Wu, Y. B. et al.** 2013. Experimental study on brittle-ductile transition in elliptical ultrasonic assisted grinding (EUAG) of monocrystal sapphire using single diamond abrasive grain. *International Journal of Machine Tools and Manufacture*, 71(8): 41-51.  
<https://doi.org/10.1016/J.IJMACTOOLS.2013.04.004>.
  3. **Li, C.; Zhang, F. H.; Meng, B.B. et al.** 2017. Material removal mechanism and grinding force modelling of ultrasonic vibration assisted grinding for SiC ceramics. *Ceramics International*, 43(3): 2981-2993.  
<http://dx.doi.org/10.1016/j.ijmachtools.2013.04.004>.
  4. **Liu, L. F.; Zhang, F. H.; Liu, M. H.** 2015. Ultrasonic assisted grinding for silicon carbide. *Optics and Precision Engineering*, 23(8): 2229-2235.  
<http://dx.doi.org/10.3788/ope.20152308.2229>.
  5. **Fu, P.; Yang, W. P.; Wu, Y. B.** 2018. Investigation of silicon wafer surface morphology and roughness processed by fixed abrasive polishing with assistance of ultrasonic vibration. *Journal of Vibration and Shock*, 37(24): 237-243.  
<http://dx.doi.org/10.13465/j.cnki.jvs.2018.24.035>.
  6. **Chen, C.X.; Yang, W.; Zhu, F. W.** 2023. Characteristics of textured polishing wheels for dry fixed abrasive polishing fused silica. *Applied Optics*, 62(21):5644-5651.  
<https://doi.org/10.1364/AO.497145>.
  7. **Li, X.A.; Peng, X.Q.; Hu, H.** 2016. Principle Analysis and Experimental Study of Vibration Assisted Polishing. *Aviation Precision Manufacturing Technology*, 52(4): 14-19.  
<https://doi.org/10.3969/j.issn.1003-5451.2016.04.004>.
  8. **Zhang, X.Y.; Guo, X.C.; Wang, H.; et al.** 2023. Insight into Polishing Slurry and Material Removal Mechanism of Photoassisted Chemical Mechanical Polishing of YAG Crystals. *Langmuir*, 39(38): 13668-13677.  
<https://doi.org/10.1021/acs.langmuir.3c01824>.
  9. **Chen, T.; Liu, D. F.; She, Y. X. et al.** 2016. Ultrasonic elliptical vibration-assisted chemical mechanic polishing for fiber array. *China Surface Engineering*, 29(3): 132-138.  
<https://doi.org/10.11933/j.issn.1007-9289.2016.03.018>.
  10. **Guo, J.; Feng, W. H.; Jong, H. J. H. et al.** 2020. Finishing of rectangular microfeatures by localized vibration-assisted magnetic abrasive polishing method. *Journal of Manufacturing Processes*, 49(49): 204-213.  
<https://dx.doi.org/10.1016/j.jmapro.2019.11.026>.
  11. **Guo, J.; Jong, H.J.H.; Kang, R.K.; et al.** 2018. Novel localized vibration-assisted magnetic abrasive polishing method using loose abrasives for V-groove and Fresnel optics finishing. *Optics express*, 2018, 26(9):11608-11619.  
<https://doi.org/10.1364/OE.26.011608>.
  12. **Yu, T. B.; Guo, X. P.; Wang, Z. H. et al.** 2019. Effects of the ultrasonic vibration field on polishing process of nickel-based alloy Inconel718. *Journal of Materials Processing*, 273(273): 3-11.  
<https://doi.org/10.1016/j.jmatprotec.2019.05.009>.
  13. **Yu, T. B.; Yang, X. Z.; An, J. H. et al.** 2018. Material removal mechanism of two-dimensional ultrasonic vibration assisted polishing Inconel718 nickel-based alloy. *Chemicals & Chemistry*, 96(1): 657-667.  
<https://doi.org/10.1007/s00170-018-1609-6>.
  14. **Zhao, Q.L.; Sun, Z.Y.; Guo, B.** 2017. Ultrasonic vibration-assisted polishing of V-groove arrays on hard and brittle materials. *Proceedings of the Institution of Mechanical Engineers*, 231(2): 346-354.  
<https://doi.org/10.1177/0954405415616789>.
  15. **Zhao, Q.L.; Sun, Z.Y.; Guo, B.** 2016. Material removal mechanism in ultrasonic vibration assisted polishing of micro cylindrical surface on SiC. *International Journal of Machine Tools and Manufacture*, 103(103): 28-39.  
<https://dx.doi.org/10.1016/j.ijmachtools.2016.01.003>.
  16. **Xu, W. H.; Lu, X. C.; Pan, G.S. et al.** 2010. Ultrasonic flexural vibration assisted chemical mechanical polishing for sapphire substrate. *Applied Surface Science*, 256(12): 3936-3940.  
<https://doi.org/10.1016/j.apsusc.2010.01.053>.

R. Niu, H. Wang, Z. Wu, L. Sun

#### EFFECT OF VIBRATION DIRECTION ON VIBRATION-ASSISTED FIXED ABRASIVE POLISHING

#### S u m m a r y

In order to study the effect of vibration direction on vibration-assisted fixed abrasive polishing and explore the influence rule of vibration direction on material removal rate and workpiece surface quality, a single abrasive particle vibration-assisted fixed abrasive polishing model was established to study the effect of axial and radial vibration on workpiece profile depth, surface morphology, etc. And the experiments of vibration-assisted fixed abrasive polishing in different vibration directions were carried out. The results show that axial vibration auxiliary polishing can greatly advance the processing efficiency, and improve the workpiece material removal rate by 27.6%; radial vibration auxiliary polishing can achieve better surface quality, and reduces the surface roughness by 59.8%.

**Keywords:** fixed abrasive polishing, vibration direction, vibration-assisted polishing, material removal rate, surface quality.

Received April 26, 2023

Accepted February 15, 2024



This article is an Open Access article distributed under the terms and conditions of the Creative Commons Attribution 4.0 (CC BY 4.0) License (<http://creativecommons.org/licenses/by/4.0/>).